Identification of a Peptide Toxin from *Grammostola spatulata* Spider Venom that Blocks Cation-selective Stretch-activated Channels

Thomas M. Suchyna,* Janice H. Johnson,‡ Katherine Hamer,‡ Joseph F. Leykam,§ Douglas A. Gage,§ Henry F. Clemo,‖ Clive M. Baumgarten,‖ and Frederick Sachs*

From the *Department of Physiology and Biophysics, State University of New York at Buffalo, Buffalo, New York 14214; ‡NPS Pharmaceuticals, Inc., Salt Lake City, Utah 84108; ‖Department of Internal Medicine and Physiology, Medical College of Virginia, Virginia Commonwealth University, Richmond, Virginia 23298; and §Department of Biochemistry, Michigan State University–National Institutes of Health Mass Spectrometry Facility, Michigan State University, East Lansing, Michigan 48824-1319

abstract We have identified a 35 amino acid peptide toxin of the inhibitor cysteine knot family that blocks cationic stretch-activated ion channels. The toxin, denoted GsMTx-4, was isolated from the venom of the spider *Grammostola spatulata* and has <50% homology to other neuroactive peptides. It was isolated by fractionating whole venom using reverse phase HPLC, and then assaying fractions on stretch-activated channels (SACs) in outside-out patches from adult rat astrocytes. Although the channel gating kinetics were different between cell-attached and outside-out patches, the properties associated with the channel pore, such as selectivity for alkali cations, conductance (~45 pS at −100 mV) and a mild rectification were unaffected by outside-out formation. GsMTx-4 produced a complete block of SACs in outside-out patches and appeared specific since it had no effect on whole-cell voltage-sensitive currents. The equilibrium dissociation constant of ~630 nM was calculated from the ratio of association and dissociation rate constants. In hypotonically swollen astrocytes, GsMTx-4 produces ~40% reduction in swelling-activated whole-cell current. Similarly, in isolated ventricular cells from a rabbit dilated cardiomyopathy model, GsMTx-4 produced a near complete block of the volume-sensitive cation-selective current, but did not affect the anion current. In the myopathic heart cells, where the swell-induced current is tonically active, GsMTx-4 also reduced the cell size. This is the first report of a peptide toxin that specifically blocks stretch-activated currents. The toxin affect on swelling-activated whole-cell currents implicates SACs in volume regulation.

key words: mechanogated • swell • astrocyte • ventricular • myocytes

INTRODUCTION

High-affinity inhibitory peptide toxins have proven to be powerful tools for elucidating the ion channel components of whole-cell currents. Stretch-activated channels (SACs)[1] are the only major class of ion channels for which a specific inhibitor does not exist. Gd^{3+} is the best known blocker of SACs (K_ds ranging from 1 to 100 μM) and is widely used to identify these channels. However, Gd^{3+} also blocks a variety of other channels such as L- and T-type Ca^{2+} (Biagi and Enyeart, 1990), K^+ delayed rectifier, voltage-gated Na^+ (Elinder and Arhem, 1994), and Ca^{2+} ER release channels (Kluesener et al., 1995). Also, a variety of "specific" blockers for voltage- and ligand-gated channels (e.g., amiloride, cationic antiobiotics, tetrodotoxin, tetraethylammonium, quinidine, diltiazem, and verapamil) exhibit low affinity blocking activity against SACs (for review, see Hamill and McBride, 1996; Sachs and Morris, 1998).

SACs have been implicated as either activators or modifiers of many different cellular responses to mechanical stimuli, including modification of electrical and contractile activity of muscle tissue, involvement in volume regulatory ion fluxes, and initiation of action potentials in specialized sensory cells such as inner hair cells of the cochlea and Merkel cells in the epithelium (Sachs, 1992; Sachs and Morris, 1998; Tazaki and Suzuki, 1998). However, it has proven difficult to definitively associate mechanically stimulated physiological responses with specific SACs in the absence of an inhibitor.

This limitation is nowhere more evident than in volume regulation studies, where cells undergo a regulated volume decrease (RVD) in response to hypotonic stress. RVD is produced by efflux of cytoplasmic inorganic osmolytes (mainly K^+ and Cl^-) and small organic molecules. K^+ and Cl^- efflux occurs via cotransporters and individual conductive channels that are separate, but interdependent (for reviews, see Chamberlin and Strange, 1989; Hoffmann and Simonsen, 1989; Sarkadi and Parker, 1991; Pasantes-Morales, 1996). RVD in astrocytes has been intensely studied due to its impor-

Address correspondence to Thomas M. Suchyna, Dept. of Physiology and Biophysics, 320 Cary Hall, SUNY at Buffalo, Buffalo, NY 14214. Fax: 716-829-2028; E-mail: suchyna@acsu.buffalo.edu

[1]*Abbreviations used in this paper:* CHF, congestive heart failure; DIDS, 4,4′-diisothiocyanatostilbene-2,2′-disulphonic acid; ICK, inhibitor cysteine knot; RP, reverse phase; RVD, regulated volume decrease; SAC, stretch-activated channel; TFA, trifluoroacetic acid.

tance in controlling brain edema (Kimelberg, 1995; Pasantes-Morales, 1996). These cells display a fast RVD response and possess a high resting K^+ flux. Within the first minute after hypotonic swelling of neonatal astrocytes (~160 mOsM reduction), the membrane potential depolarizes by ~50 mV (Kimelberg et al., 1990). The depolarization is primarily caused by a rapidly activated 4,4′-diisothiocyanatostilbene-2,2′-disulphonic acid (DIDS)–sensitive anion current (Pasantes-Morales et al., 1994; Bakhramov et al., 1995). There is also a Ca^{2+} influx during hyposmotic swelling that is partially mediated by opening of dihydropyridine-sensitive Ca^{2+} channels (O'Connor and Kimelberg, 1993; Bender et al., 1994). It is important to remember that most agents purported to be specific, such as dihydropyridines, have not been tested against SACs.

A number of studies have suggested that nonselective cation-permeable SACs play a role in both membrane depolarization (Kimelberg and Kettenmann, 1990) and Ca^{2+} influx observed during RVD (Christensen, 1987; O'Connor and Kimelberg, 1993; Chen et al., 1996). In addition, K^+-selective SACs and a curvature-sensitive nonselective cation channel have been described in neonatal astrocyte cultures (Bowman et al., 1992; Islas et al., 1993). A cation-selective SAC has also been identified in C6 glioma cells (Bowman and Lohr, 1996). However, none of these channels have been investigated for involvement in RVD.

SACs have also been implicated in mechanical sensitivity of the heart. Mechanical stimulation of cardiac myocytes and whole heart preparations can cause depolarization, extrasystoles, and arrhythmias (see Hu and Sachs, 1997). Also, chronic hemodynamic stress that leads to congestive heart failure (CHF) and the accompanying cellular hypertrophy may be initiated by stretch- or swelling-activated currents (Sachs, 1988; Vandenberg et al., 1996; Clemo and Baumgarten, 1997). CHF chronically activates a whole-cell cation-selective current previously identified with hypotonic swelling or chronic rapid pacing (Clemo et al., 1998). A blocker of SACs could have clinical use.

Chen et al. (1996) showed that crude *Grammostola* venom could block SACs in an outside-out patch from GH3 pituitary cells. They also demonstrated the venom can block Ca^{2+} uptake during hypotonic swelling, but not during high K^+ depolarization, which would activate voltage-gated Ca^{2+} channels. Thus, it was suggested that Ca^{2+} uptake was triggered by the activation of SACs. The primary aim of this study was to isolate and characterize the active component from *Grammostola* venom.

To isolate this SAC-blocking component(s), fractions of the venom were screened by perfusion onto outside-out patches from adult rat astrocytes, a preparation in which SACs could be maintained active. A single component peak was identified and sequenced, revealing a unique peptide (noted GsMTx-4) containing an inhibitor cysteine knot (ICK) consensus motif (Narasimhan et al., 1994). The toxin exhibited negligible activity against voltage-sensitive whole-cell currents. However, the toxin did reduce swelling-activated whole-cell currents in astrocytes and CHF model cardiac myocytes. The effect of this new toxin on whole-cell currents, for the first time, directly implicates specific cation-selective SACs in the response to swelling.

METHODS

Toxin Isolation

Grammostola spatulata (Theraphosidae) spiders were obtained from a captive population at Hogel Zoo (Salt Lake City, UT). The *Grammostola* species have recently been reassigned to the genus *Phixotricus* (Perez et al., 1996), but *Grammostola* is used here to maintain consistency with earlier biomedical publications. Venom was collected by an electrical milking procedure (Bascur et al., 1982) and stored at −80°C. It was fractionated by high-performance liquid chromatography, incorporating Beckman System Gold 126 solvent delivery and 168 photodiode-array detector modules (Beckman Instruments, Inc.), and using linear gradients with a flow rate of 3.5 ml/min unless noted. Whole venom (825 μl) was separated into eleven 75-μl aliquots that were each diluted to 2 ml each with 15% solvent B. Solvent A was 0.1% trifluoroacetic acid (TFA) in water and solvent B was 0.1% TFA in acetonitrile. The diluted venom was fractionated on a Zorbax RX-C8 (9.4 × 250 mm, 5 μm, 300 Å; Mac-Mod Analytical, Inc.) reversed-phase (RP) column equilibrated in 15% solvent B. The column was developed with a 40-min gradient (15–55% solvent B) begun 3 min after injection of the sample with a flow of 3.5 ml/min. The effluent was monitored at 280 nm and fractions were collected as noted on the chromatogram (see Fig. 3 A). Similar fractions from all 11 chromatographies were combined, lyophilized, and tested for bioactivity. The assay samples were dissolved in 140 mM NaCl, 10 mM HEPES, 5 mM KCl, 2 mM $MgSO_4$, to a final dilution of 1:1,000, relative to whole venom, for testing on outside-out patches. Several of the pools showed partial block of the SACs (as described below), but only pool 9 gave consistent, complete block of the channels.

Further purification of pool 9 (see Fig. 4 B) was achieved by RP chromatography on a Vydac C18 column (10 × 250 mm, 5 μm, 300 Å; The Separations Group) equilibrated in 10% solution B. Lyophilized pool 9 was dissolved in 4 ml of 10% solution B and chromatographed in 1-ml portions eluting with a 10-min gradient (10–28% solution B), followed by a 64-min gradient (28–60% solution B). The first gradient was begun 5 min after injection of the sample, the effluent was monitored at 220 nm, and three fractions were collected. Corresponding fractions from the four chromatographies were combined, lyophilized, and assayed as described above. Only pool B showed block of the SACs.

Attempts to affect further purification of pool B by anion and cation exchange chromatography (MonoQ and MonoS resins; Pharmacia LKB Laboratories, Inc.) were unsuccessful. The material was not retained on the anion exchange column and retained too strongly on the cation exchange columns. The peptide did not elute with salt gradient from any of the cation exchange resins tried (0–2 M NaCl in 50 mM sodium phosphate buffer, pH 7.0). A broad peak of material did elute at ~pH 11 from the MonoS column with a gradient from pH 7–12 (50 mM sodium phosphate buffer, 0.1 M in NaCl), but no resolution from other components was visible.

Therefore, pool B was subjected to a final RP chromatography to remove a small amount of earlier and later eluting peptides. Pool B was diluted to 4 ml with 20% solvent B and 0.5-ml portions chromatographed on the Zorbax column described above, eluting with a 7-min gradient (20–27% solution B), followed by a 46-min gradient (27–50% solution B), and the effluent was monitored at 220 nm (see Fig. 3 C). The first gradient was begun 5 min after injection of the sample. The active peptide, GsMTx-4, eluted between 29.5 and 30.5 min. Corresponding fractions from the eight chromatographies were pooled to give 7.5 mg of GsMTx-4. The average yield of GsMtx-4 from several purifications was 8 mg/ml of venom fractionated, which implies that the toxin is ~2 mM in whole venom. The purity of the final product used in single channel and whole cell assays was assessed by analytical chromatography on an Aquapore RP300 C8 column (4.6 × 220 mm, 7 μm, 300 Å; PE Biosystems), eluting with a 25-min linear gradient (32–47% solution B) with a flow of 1 ml/min monitored at 220 nm (see Fig. 3 D). Elution with a gradient of methanol/water (0.1% in TFA) gave a similar profile with a longer retention time, but revealed no other impurities.

Mass Spectrometry

1 μl of the sample solutions (intact toxin or fragments) in 0.1% TFA (or the HPLC elution solvent) were mixed on the sample plate with 1 μl of a saturated solution of 4-hydroxy-α-cyanocinnamic acid in 1:1 CH_3CN:0.1% aqueous TFA. The solution was allowed to air dry before being introduced into the mass spectrometer. Spectra were acquired on a PerSeptive Biosystems Voyager Elite MALDI-TOF (matrix-assisted laser desorption ionization–time of flight) instrument operated in linear delayed extraction mode (50–100 ns). The instrument was equipped with a nitrogen laser (3-ns pulse). The acceleration potential was 22 kV.

Sequencing

The toxin was further purified by microbore RP-HPLC (0.8 × 250 mm C18 column, with a linear gradient from 0.1% TFA-15% CH_3CN to 0.1% TFA-70% CH_3CN in 90 min, flow rate 40 μl/min, monitored at 214 nm). The toxin peak was collected at 24.6 min. The HPLC fraction (~1 nmol) was dried down and taken up in 80 μl 8-M guanidine HCL-100 mM Tris-5 mM tributylphosphine, pH 8.5, and incubated for 8 h at 55°C. *N*-Isopropyliodoactamide (1 mg in 20 μl MeOH + 80 μl Tris) was added and the solution was incubated for an additional 2 h at room temperature. The reduced and alkylated peptide was then desalted by HPLC on a C18 column as described above (elution time, 30.1 min). NH_2-terminal sequencing was carried out on an ABI 477 after loading the reduced and alkylated peptide on PVDF membrane.

Digestion with BNPS [(2-2-nitrophenylsulfenyl)-3-methyl-3-bromoindolenine]-skatole (Fontana, 1972) was carried out by dissolving the purified reduced and alkylated peptide in 50 μl 0.1% TFA and 15 μl BNPS-skatole. The solution was incubated at room temperature for 8 h. The digestion products were separated by HPLC as described above. Two main peaks were collected and sequenced by Edman degradation. Asp-N digestion (Wilson, 1989) was performed by dissolving the purified reduced and alkylated peptide in 100 mM Tris, pH 8.0 and treating with 1% (wt/wt) Asp-N for 20 h at 35°C. The fragments were separated and analyzed by mass spectrometry before Edman degradation.

Astrocyte Cell Culture

Activated adult astrocytes, isolated from gelatin-sponge implants from adult Sprague-Dawley rat brains (Langan et al., 1995), were provided courtesy of Dr. Thomas Langan (SUNY Buffalo, Buffalo, NY) at passages 2–4. Astrocytes were maintained in DMEM, 10% fetal bovine serum, and 1% penicillin/streptomycin and were used in experiments between 2 and 5 d after passage. Cells between passages 4 and 35 expressed SACs with the same properties. Both stellate and polygonal (fibroblast-like) cells were used.

Astrocyte Single-Channel Patch Clamp

Patch voltage was controlled by an Axopatch 200B (Axon Instruments) and stored directly on computer disk via a Labmaster DMA version B (Scientific Instruments) board controlled by pClamp6-Clampex acquisition software (Axon Instruments). Currents were sampled at 10 kHz and low-pass filtered at 2 kHz through a four-pole Bessel filter on the Axopatch 200B. Experimental voltage protocols were controlled by pClamp6-Clampex. All potentials are defined with respect to the extracellular surface.

Electrodes were pulled on a pipette puller (PC-84; Brown-Flaming Instruments), painted with Sylgard 184 (Dow Corning Corp.) and fire polished. Electrodes were filled with KCl saline containing (mM): 140 KCl, 5 EGTA, 2 $MgSO_4$, 10 HEPES, pH 7.3) and had resistances ranging from 3 to 8 MΩ. Bath saline consisted of (mM): 140 NaCl, 5 KCl, 1 $MgSO_4$, 1 $CaCl_2$, 6 glucose, and 10 HEPES, pH 7.3.

Pressure and suction were applied to the pipette by a pressure clamp designed and constructed in our laboratory by Dr. Steven Besch. Pressure values refer to pressure in the pipette; i.e., the intracellular side of the membrane in outside-out patches. Suction applied to a cell-attached patch has the same sign as pressure applied to an outside-out patch. The rise time of pressure changes at the tip were determined by monitoring the rate of current change when pressure steps were applied to an electrode containing 150 mM KCl solution and placed in a water bath. The τ_{10-90} was ~5 ms, as determined by exponential fits to the current decay. Perfusion of the patch was handled by a pressurized bath perfusion system with eight separate channels (BPS-8; ALA Scientific).

Offline data analysis was performed with pClamp6 analysis software and Origin 5.0. Maximal unitary channel currents were determined via Gaussian fits to the peaks of the all-points amplitude histograms from records containing one to three channels. Many current records displayed more than three channel openings (maximal single channel currents plus subconductance states) and were impossible to fit using Pstat software. Some of these records were analyzed by determining all step-like changes in the current during the pressure application and selecting the average maximal current level as the unitary current. The data analyzed by this method was in good agreement with the unitary current levels determined by analysis of all points amplitude histograms from single-channel patches.

Astrocyte Whole-Cell Current Clamp

Whole-cell current was measured by the Nystatin-perforated patch technique (Horn and Marty, 1988). Bath saline was the same as above. Pipette saline consisted of (mM): 80 KCl, 30 K_2SO_4, 10 NaCl, 3 $MgSO_4$, 0.13 $CaCl_2$, 0.23 EGTA, and 10 HEPES, pH 7.3. Nystatin was dissolved in pipette saline to a final concentration of 200 μg/ml. After patch formation, access resistance was allowed to drop to ~15 MΩ (uncompensated), after which the series resistance compensation was set at ~65%, and prediction was set to ~75%. Whole-cell capacitance measurements ranged from ~25 to 50 pF. Whole-cell currents were monitored by either a voltage-step protocol (see Fig. 9), or by 600-ms voltage ramps. During hypotonic swelling, the cell was perfused initially with isotonic saline (bath saline with 160 mM mannitol replacing 80 mM NaCl) before switching to hypotonic saline (isotonic saline minus 140 mM mannitol). The BPS-8 perfusion system described above was used to rapidly (<200 ms) change the bathing solution. Peak currents were measured at 3–5 ms into voltage steps.

Cardiac Myocyte Preparation

Ventricular myocytes were freshly isolated from New Zealand white rabbits with aortic regurgitation-induced congestive heart failure (Magid et al., 1988) using a collagenase–pronase dispersion method (Clemo and Baumgarten, 1997). Cells were stored in a modified Kraft-Bruhe solution containing (mM): 132 KOH, 120 glutamic acid, 2.5 KCl, 10 KH_2PO_4, 1.8 $MgSO_4$, 0.5 K_2EGTA, 11 glucose, 10 taurine, 10 HEPES, pH 7.2. Myocytes were used within 6 h of harvesting and only quiescent cells with no evidence of membrane blebbing were selected for study.

Cardiac Myocyte Electrophysiology and Volume Determination

For a detailed explanation of methods, see Clemo and Baumgarten (1997). In brief, electrodes were pulled from glass capillaries to give a final tip diameter of 3–4 μm and a resistance of 0.5–1 MΩ when filled with the standard electrode filling solution containing (mM): 120 K aspartate, 10 KCl, 10 NaCl, 3 $MgSO_4$, 10 HEPES, pH 7.1. Whole-cell currents were recorded using an Axoclamp 200A. Pulse and ramp protocols, voltage-clamp data acquisition, and offline data analysis were controlled with custom programs written in ASYST. Both step and ramp voltage-clamp protocols were applied with a holding potential of −80 mV. Currents were digitized at 1 kHz and low-pass filtered at 200 Hz. Whole-cell currents were recorded using the amphotericin perforated-patch technique. Solution changes were performed by bath perfusion that was completed within 10 s. The standard bath solution contained (mM): 65 NaCl, 5 KCl, 2.5 $CaSO_4$, 0.5 $MgSO_4$, 10 glucose, and 10 HEPES, pH 7.2, and 130 (1T) or 283 (1.5T) mannitol to control the osmolarity. Isotonic osmolarity was taken as 296 (1T) and 444 (1.5T) mosm for hypertonic solution. Myocyte volume was determined by visualization with an inverted microscope (Diaphot; Nikon Inc.) equipped with Hoffman modulation optics and a high-resolution TV camera coupled to a video frame grabber. Images were captured online each time a ramp or step voltage-clamp protocol was performed using a program written in C and assembler and linked to ASYST voltage-clamp software. A combination of commercial (MOCHA; SPSS Inc.) and custom (ASYST) programs were used to determine cell width, length, and area of the image.

RESULTS

SAC Properties in Activated Adult Rat Astrocytes: Cell-attached Versus Outside-Out

The most efficient method for screening multiple venom samples is to use outside-out patches. However, first it was necessary to show that SAC function is maintained in the outside-out patch configuration. To date, all studies investigating the properties and function of SACs in astrocytes have focused on neonatal preparations and C6 glioma cell lines (Bowman et al., 1992; Bowman and Lohr, 1996; Islas et al., 1993) due to difficulties in culturing adult astrocytes. Langan et al. (1995) showed that adult-activated rat astrocytes from gel foam implants could be isolated and cultured through >10 passages, while maintaining all type 1 astrocytic markers [glial fibrillary acidic protein (GFAP), vimentin, 7B11, and RAN2], contact inhibition, and cell cycle kinetics. In cell-attached patches, activated adult astrocytes express primarily one type of SAC that can be activated by both pressure and suction (Fig. 1 A, only pressure data shown). Observation from >100 patches typically showed two to five channels/patch. Consistent with the results of Hamil and McBride (1992) and Small and Morris (1995), SAC activity in cell-attached patches was sensitive to the level of suction used in seal formation. Channels were rarely observed when >10 mmHg of suction was used during seal formation, whereas >90% of patches showed channel activity with <10 mmHg. With 140 mM KCl in the electrode, the single-channel conductance inwardly rectified being 46 pS at −100 mV, but only 21 pS at +100 mV (Fig. 1 C). Channel activity was normally initiated by applying between 25 and 35 mmHg of suction. However, rundown did occur so that increasing levels of suction were required to activate the channels over the 5–10 min during which data was acquired.

The open probability (P_o) was time and voltage dependent, displaying a fast adaptation (within 100 ms at hyperpolarized potentials) similar to that reported for *Xenopus* oocytes (Hamill and McBride, 1992). The time dependence of P_o can be described by an initial phasic period followed by a tonic period, as defined in Bowman and Lohr (1996). Both the duration of the phasic period and P_o during the tonic period showed a steep voltage dependence, decreasing as the potential became more negative (Fig. 1 A, see average currents). Of 16 cell-attached patches analyzed, 12 displayed adaptation at hyperpolarized potentials. In addition to adaptation, multiple voltage-dependent substates were visible at −100 mV, compared with only one at depolarizing potentials. Kinetic analysis of these substates is currently in progress. One major subconductance state observed at positive potentials (not shown in this figure) was 80–90% of the maximal conductance state, similar to that reported in *Xenopus* oocytes (Silberberg and Magleby, 1997). Adaptation was also observed in C6 glioma cells (Bowman and Lohr, 1996). However, in contrast to the rapid adaptation observed in adult astrocytes, adaptation in C6 cells occurred over 1–2 s and was not as strongly voltage dependent.

Channel activity in outside-out patches was generally similar to that in cell-attached patches, but they had different adaptation properties (Fig. 1 B). The SACs opened in response to both pressure and suction. With 140 mM KCl in both the pipette and the bath, the I-V profile (44 pS at −100 mV, and 21 pS at +100 mV, cytoplasmic side) was nearly identical to that observed for cell-attached patches (Fig. 1 D). In this configuration, the channels were initially activated by between 30 and 40 mmHg of pressure. The similarities between the conductance and pressure sensitivity in the two patch configurations suggest that these channel properties have not been significantly modified by outside-out patch formation. However, of 12 outside-out patches, only one displayed the fast adaptation property ob-

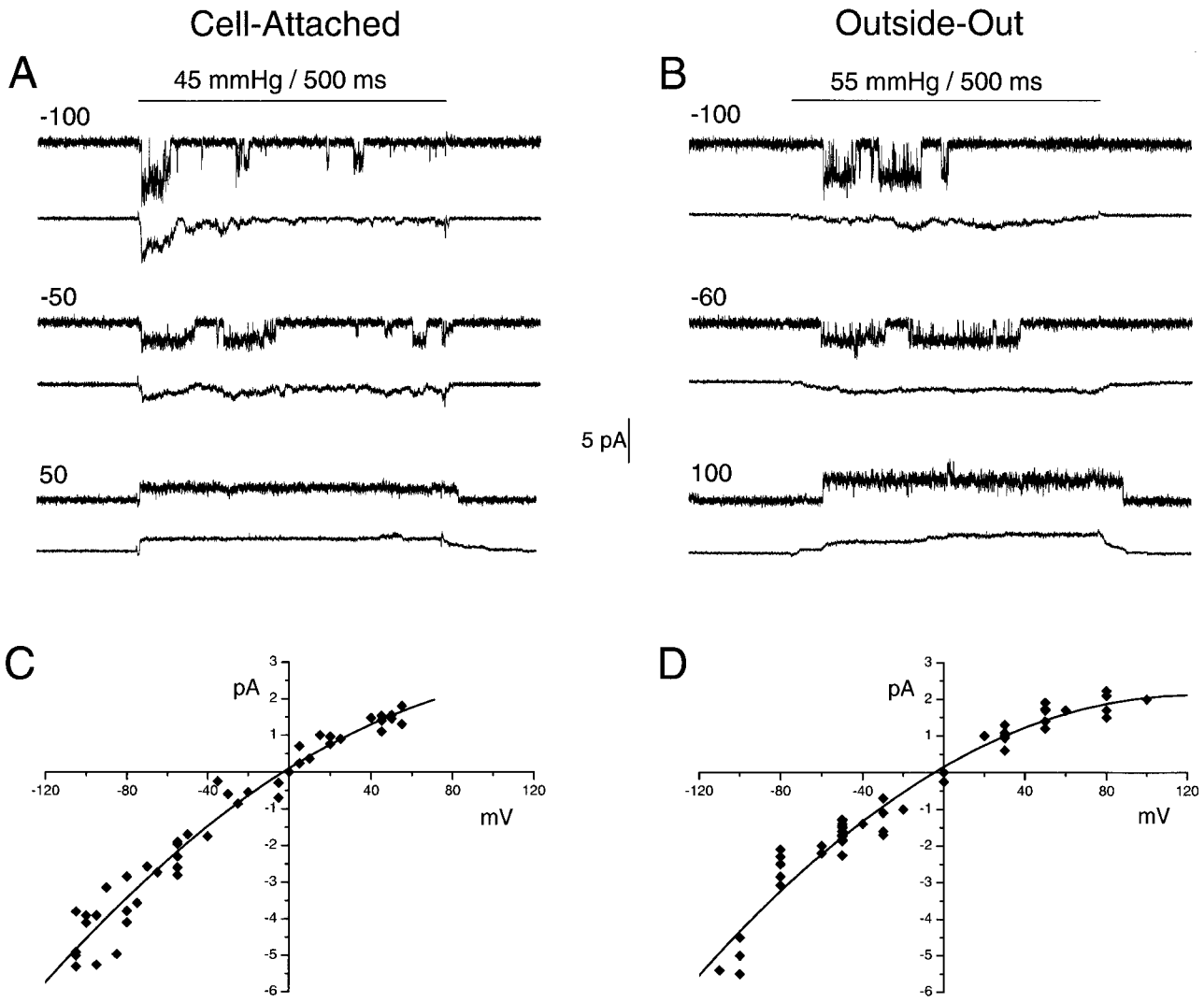

Figure 1. Cell-attached and outside-out patches from adult activated astrocytes showing stretch-sensitive channels with similar unitary conductance profiles but different gating properties. Representative single-channel current recordings are shown above average patch currents from a cell-attached patch (A) containing a single channel, and an outside-out patch (B) containing two to three channels. Cell-attached patch recordings were made with 140 mM KCl pipette saline, and outside-out patch recordings are with symmetrical 140-mM KCl pipette solutions. Pressure steps (indicated by the bar at the top) were applied to the patches at different holding potentials shown to the left of each recording. Voltages are relative to the extracellular side. Average current records were calculated from multiple pressure steps (ranging from 5 to 15 steps) at each voltage. In cell-attached mode, channel adaptation, lower P_o, and multiple subconductance states are apparent at negative potentials. Channels in outside-out patches from astrocytes show slow voltage-dependent activation and lower P_o at negative potentials. Unitary current–voltage plots were fitted with a second-order polynomial and show inward rectification for channels in cell-attached (C, $n = 11$) and outside-out (D, $n = 16$) patches. Voltages for cell-attached data points were corrected for the average resting membrane potential measured in the whole cell configuration. Each point represents an average current calculated by applying multiple pressure steps to a single patch.

served in cell-attached patches. Instead, two showed no change in P_o with respect to time or voltage, while the remaining nine patches exhibited a slow increase in current at both positive and negative voltages, where the number of active channels increased during the 500-ms pressure step (Fig. 1 B, 100 mV, and see Fig. 5 A, average control current). The rate of increase was greater for pressure steps at positive voltages due to an increase in P_o at positive potentials. Similar responses are observed in *Xenopus* oocytes when large pressure stimuli are applied to eliminate the adaptation property (see Figure 2 in Hamill and McBride, 1992). Outside-out formation is likely to disrupt the associations between membrane and cytoplasmic attachments in a similar way to the high pressure stimuli applied to cell-attached patches of the *Xenopus* oocyte.

The single channel conductance and inward rectification observed here were similar to the properties reported for other members of the family of nonselective cation SACs (for review, see Yang and Sachs, 1993).

Like other nonselective SACs, the astrocyte channels were not blocked by 130 mM Cs^+ (data not shown). The channels were cation selective based on external ion substitution experiments with outside-out patches. When gluconate (Fig. 2, ◆) was substituted for Cl^- (□), we saw no change in the I-V profile. However, substituting $NMDG^+$ (▼) for K^+ in the bath produced an 88% reduction in current at −100 mV. The channel displayed a weak selectivity for K^+ over Na^+ since the current was reduced 24% at −100 mV when Na^+ was substituted for K^+ in the bath (Fig. 2, △). The properties of this SAC in adult astrocytes were similar to the cation-selective SACs described for many other cell types, including C6 glioma cells. SACs in C6 cells display a unitary conductance of 40 pS in equimolar 100-mM KCl are inwardly rectifying and show voltage-dependent adaptation (Bowman and Lohr, 1996). However, SACs in our adult astrocyte differed from the highly K^+-selective channels (Islas et al., 1993) and from the ~50-pS curvature-sensitive channels (Bowman et al., 1992) reported in neonatal astrocytes preparations.9

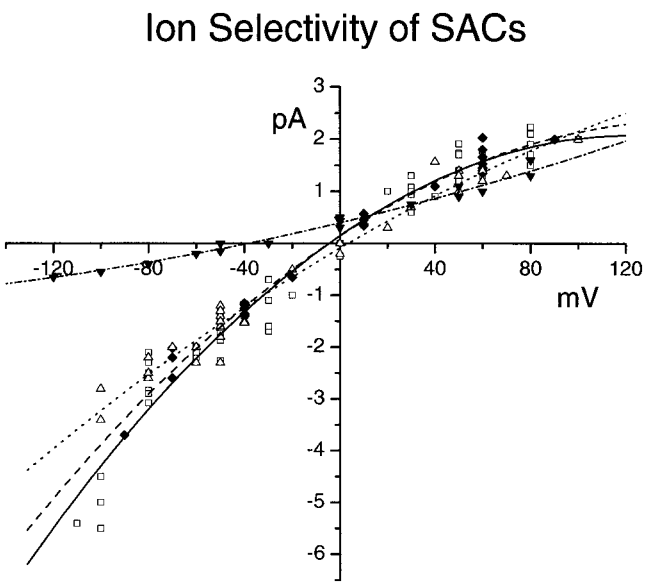

Figure 2. External ion substitution shows SACs are cation selective in outside-out patches. The pipette saline was 140 mM KCl. Each data point represents the average current from multiple pressure steps to a single patch. The data sets were fitted with second-order polynomials. Data for symmetrical 140 mM KCl (□, solid line fit) are the same as shown in Fig. 1 D. Switching from 140 mM KCl to 140 mM NaCl (△, dotted line fit) in the bath reduced the conductance at −100 mV from 44 to 33 pS, while there was no change in conductance at +100 mV (n = 10 patches). This suggests a weak selectivity for K^+ over Na^+. When external Cl^- is replaced with a less permeable anion gluconate (◆, dashed line fit), there was a negligible reduction in conductance at −100 mV (41 pS), and no change in conductance at +100 mV (n = 4 patches). However, when external K^+ is replaced with the impermeant cation NMDG (▼, dash-dot line fit), the conductance was reduced to 5 pS at −100 mV (n = 3 patches).

Astrocyte SAC Pharmacology

To characterize the SACs of adult astrocyte, we examined a number of compounds purported to be active against SACs in other systems (Table I). Gd^{3+}, the most commonly used SAC reagent, completely blocked the channels in adult astrocytes at 50 μM. Amiloride, which blocks epithelial Na^+ channels with nanomolar affinity, and the endogenous SACs in oocytes and audiovestibular hair cells (Jorgensen and Ohmori, 1988; Lane et al., 1991), had no effect at 20 μM.

Although NMDA-type glutamate receptors have not been observed in astrocytes, these channels do show stretch sensitivity in macropatches from neonatal neurons (Paoletti and Ascher, 1994). In neonatal astrocytes, the potent (nanomolar affinity) NMDA open-channel blocker MK801 inhibits glutamate-stimulated K^+ influx (Bender et al., 1998). Hence, we tested glutamate and MK801 on the adult astrocyte SACs. Glutamate at 10 μM did not activate SACs in unstretched patches that contained SACs, and 20 μM MK801 did not block SAC opening when stretched.

Some reports indicate that L-type Ca^{2+} channels are stretch sensitive (Langton, 1993; Ben-Tabou et al., 1994) and that blockers of these channels are active against SACs (Ruknudin et al., 1993; Small and Morris, 1995). Neither 100 μM diltiazem nor 50 μM nifedipine showed any blocking activity against the SACs in adult astrocytes. The anion channel blocker DIDS produced a significant reduction in the amount of swelling-activated anion current in astrocytoma cells (Bakhramov et al., 1995), but 50 μM DIDS had no effect on stretch-activated currents in the patch.

Identification and Characterization of a SAC Blocking Toxin from Grammostola Venom

HPLC fractions of *Grammostola* (Gs) were lyophilized, redissolved at a 1:1,000 dilution and perfused onto outside-out patches. Fraction 9, on the Gs whole-venom

TABLE I

Pharmacology of Astrocyte SACs

Compound	n	Concentration	Activity
		μM	
Gd^{+3}	2	50	Block
Amiloride	2	20	No block
MK801	2	20	No block
Glutamate	2	10	No activation
Diltiazem	3	100	No block
Nifedipine	3	50	No block
DIDS	3	50	No block

Effects of selected ion channel ligands on adult astrocyte SACs. Compounds listed were perfused, at the concentration shown, onto outside-out patches held at −50 mV, while channels were activated by pressure. *n*, number of trials.

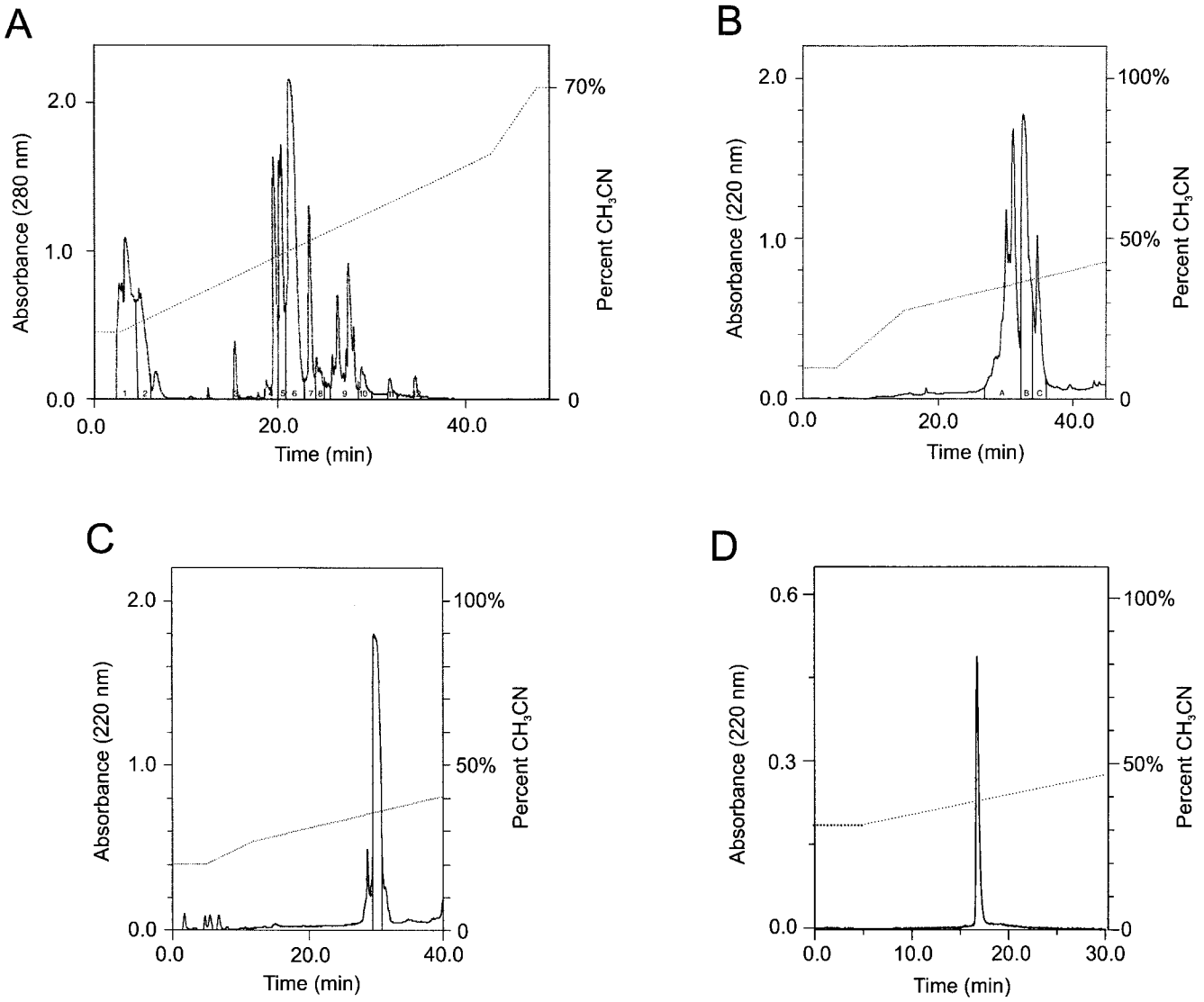

Figure 3. Reverse-phase HPLC chromatograms showing sequential purification steps for identification of GsMTx-4 peptide. The percent acetonitrile that corresponds to specific venom peaks is indicated by the dotted line shown overlaying each chromatogram. A chromatogram of *Grammostola* whole venom (A) produced by a 40-min linear gradient from 15 to 55% acetonitrile at a flow rate of 3.5 ml/min. 1–11, labeled at the bottom, designate fractions pooled for testing on outside-out patches. The lines within the chromatogram mark the boundaries of each fraction. Fraction 9 (A) contained SAC blocking activity and was further fractionated in B. (B) Only fraction B showed SAC blocking activity and was further purified in C. 10 μg of the final material used in all experiments was run on a 25-min 32–47% linear gradient of acetonitrile at a flow rate of 1 ml/min (D).

chromatogram (Fig. 3 A) blocked the SACs. This fraction was further resolved on two slower gradients (Fig. 3, B and C) at 0.5% change in acetonitrile/min until a single peptide peak was identified containing the activity (Fig. 3 D). The amount of isolated peptide was determined by weight and three different protein spectroscopic methods, showing that a 1:1,000 dilution corresponds to a concentration of 8 μg/ml whole venom. The peak was determined to have a molecular weight of 4,093.90 by mass spectrometry and designated GsMTx-4 (for *Grammostola* mechanotoxin #4). Other peptides have been isolated from Gs venom that are active against SACs (Sachs, F., unpublished observations, and GsMTx-1 U.S. Patent #5756663); however, GsMTx-4 showed the most consistent and potent activity. At this concentration, the block was complete, and occurred rapidly upon superfusion of the patch, as shown by representative current traces in Fig 4.

The association rate of the toxin was determined by applying toxin to an outside-out patch while the channels were activated by stretch. In the absence of GsMtx-4, channel activity increased over time at constant pressure (compare Fig. 1 B with 5 A). When 5 μM toxin was perfused onto the patch, 1 s after the initiation of the

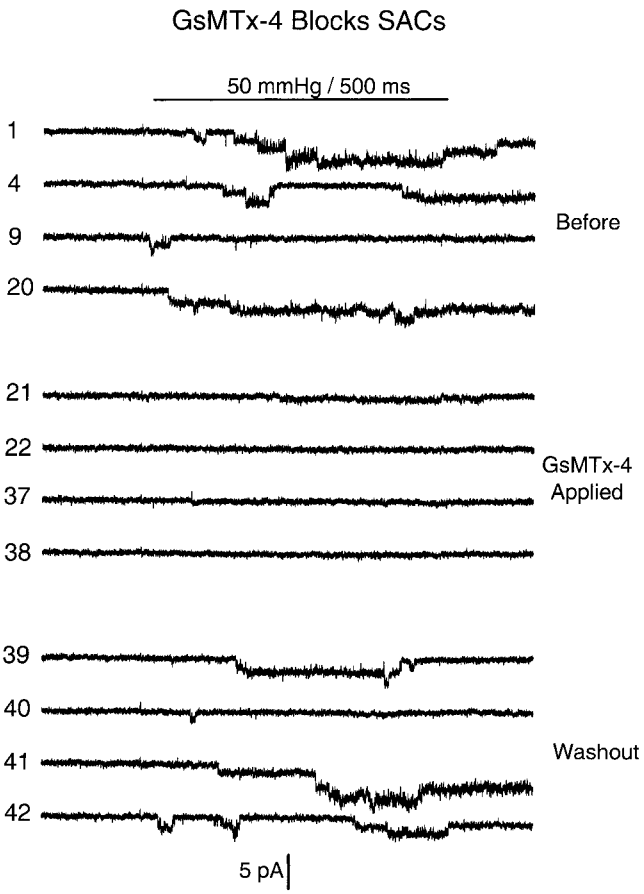

Figure 4. GsMTx-4 blocks SACs in outside-out patches. SAC activity in response to pressure steps applied to an outside-out patch before and during GsMTx-4 application, and after washout are shown. The patch was held at −50 mV, and the pressure pulse is shown above the records. The entire experiment is comprised of 60 pressure steps: steps 1–20 occur before GsMTx-4 application, 21–38 while GsMTx-4 is being perfused, and 39–60 occur during washout. Each 500-ms pressure step was separated by 1.5 s at 0 pressure. Four representative records from each stage of the experiment are displayed.

pressure step, the current decayed exponentially (Fig. 5 A, GsMTx-4). When the control and GsMTx-4 average current records are superimposed, before GsMTx-4 application, the currents are nearly identical (Fig. 5 B). The difference current was calculated (Fig. 5 C), and the period of GsMTx-4 application was fitted with a single exponential (Fig. 5 D), yielding a time constant of 594 ± 10 ms. Assuming a 1:1 binding, this gives an association constant, k_A, of $3.4 \times 10^5\ M^{-1}\ s^{-1}$.

To determine the dissociation rate, we fit the increase in average patch current ($n = 7$ patches) during toxin washout. Fit to a single exponential, the washout time constant was 4.7 ± 1.7 s (Fig. 6 B). From this dissociation constant ($k_d = 0.21\ s^{-1}$) and the association constant determined above ($k_a = 3.3 \times 10^5\ M^{-1}\ s^{-1}$), the calculated equilibrium constant, $K_d = k_d/k_a = 631 \pm 240$ nM (standard error calculated from the first-order approximation using the errors of k_a and k_d). Using the ratio of rate constants to evaluate K_d minimizes errors caused by rundown. However, the K_d calculated from the mean currents was similar. The mean SAC current was 2.04 ± 0.14 pA (SEM) over 11 pressure steps before GsMTx-4 application (Fig. 6 A), and fell to 0.17 ± 0.02 pA during toxin perfusion. (The average current over the last eight pressure steps, 10 s after GsMTx-4 washout, returned to the initial current level of 2.28 ± 0.17 pA.) For a single binding site, Michaelis-Menten kinetics predicts the ratio of the blocked to the unblocked current is $I/I_0 = 1(1 + K_d/S)$, where S is the substrate (toxin) concentration and K_d is the equilibrium dissociation constant. Using the data from Fig. 6, $I/I_0 = 0.083$, which gives a binding constant $K_d = 415$ nM, consistent with the value calculated from the ratio of association and dissociation rates.

Determining the specificity of a pharmacologic agent is an unending project, and defined only for the systems tested. We tested the pseudo–steady state I-V relationship as it related to voltage-sensitive channels. Using the perforated patch technique, 5 μM GsMTx-4 did not significantly change the I-V profile (Fig. 7 A), suggesting that it did not interact with slow, voltage-dependent, channels. By comparison, 5 mM CsCl, which was shown not to effect SACs in patches, produced a significant decrease in current at hyperpolarized potentials (Fig. 7 B), where a Cs^+-sensitive inward-rectifying K channel is known to be activated (Sontheimer, 1992).

Sequence and Disulfide Structure of GsMTx-4

MALDI-MS analysis showed the molecular weight of the native toxin was 4,093.90 (MH+ ion). The alkylated and reduced toxin displayed a peak at mass/charge 4,690, indicating three disulfide bonds or six cysteine residues were present. NH_2-terminal sequencing was followed by sequencing of two different COOH-terminal fragments produced by enzymatic digests with BNPS-skatole and Asp-N. The peptide sequence produced had a predicted mass 4,022.86, which is 71.04 D less than that measured for the intact toxin. This difference supports the presence of a COOH-terminal alanine (71.09 D), even though alanine was clearly absent in the last cycle of the Asp-N digestion product. The mass accuracy of the MALDI-MS analysis is approximately ±0.5 D with internal calibration. The final sequence shown in Fig. 8 is 35 amino acids in length with the C-term alanine added.

The six cysteine residue included in boxes form an ICK motif ($CX_{3-7}CX_{3-6}CX_{0-5}CX_{1-4}CX_{4-13}C$) commonly observed in many other peptide toxins from both terrestrial and aquatic animal venoms (Narasimhan et al., 1994; Norton and Pallaghy, 1998). GsMTx-4 shows <50% homology to any other peptide toxin. Other tarantula toxins that block voltage-gated Ca^{2+} and K^+ channels show

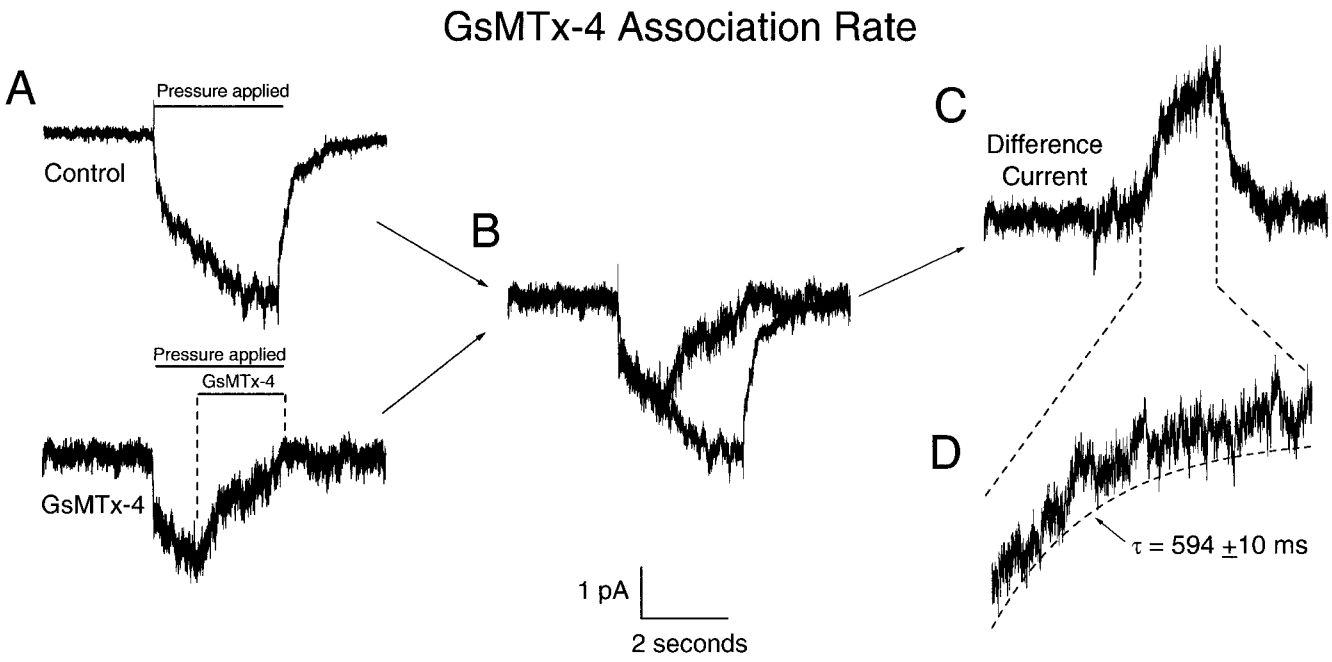

Figure 5. GsMTx-4 rate of blocking determined by superfusion of activated SACs in outside-out patches. Average SAC currents calculated from 3-s pressure steps are indicated by the bars above the traces (A). The control trace was generated from 37 pressure steps applied to seven different patches held at −50 mV, with pressure levels ranging from 35 to 70 mmHg. The current increased exponentially over the 3-s pressure application. The GsMTx-4 response was produced by applying 5 μM toxin 1 s after the onset to the pressure step indicated by the GsMTx-4 bar. The GsMTx-4 current record was averaged from 29 pressure steps to six different patches held at −50 mV, with the steps ranging between 38 and 80 mmHg. Currents were nearly identical over the first second of the average current records, as shown when the two are superimposed in B. Subtracting the control current trace from the GsMTx-4 trace produced the difference current in C. The current trace during GsMTx-4 application was fitted with a single exponential yielding a time constant of 594 ± 10 ms (D). The fit is shown displaced from the data for clarity.

the highest percentage of similarity to GsMTx-4, as illustrated by the amino acid alignment in Fig. 8. A K^+ channel toxin labeled protein 5 from *Brachypelma smithii* (Kaiser et al., 1994; Norton and Pallaghy, 1998) shows ∼50% total sequence similarity. The most significant regions of homology occur within the cysteine motif. Besides the conserved cysteine motif, there are three other residues (F4, D13, and L20) that are conserved in all five toxins. Like the positively charged ω-conotoxin and ω-agatoxin families of Ca^{2+} channel blockers, GsMTx-4 carries an overall positive charge (+5).

GsMTx-4 Effects on Astrocyte Whole-Cell Swelling-activated Currents

A large conductance increase occurs upon hypotonic swelling of neonatal astrocytes. Part of this current may

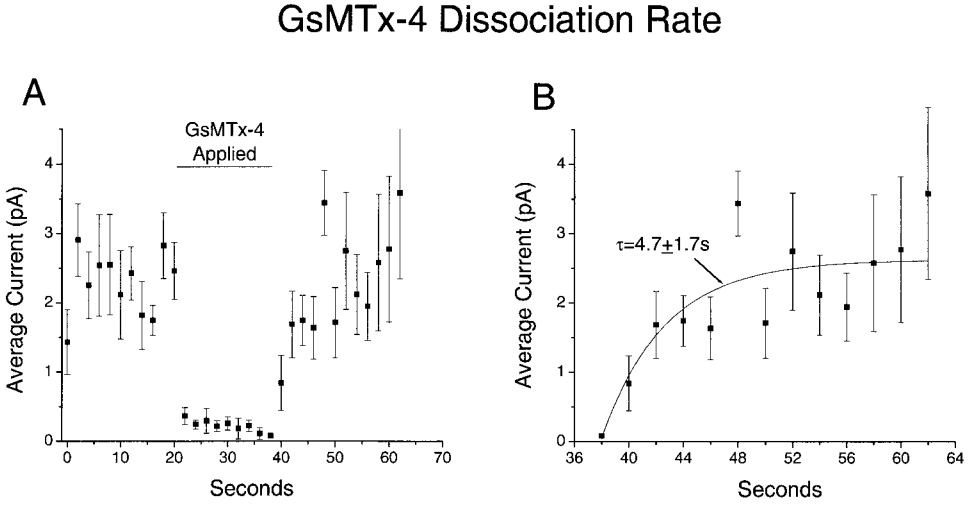

Figure 6. The GsMTx-4 dissociation rate was determined from the recovery rate of SAC current on washout. SAC currents were activated by 500-ms pressure steps at 2-s intervals in outside-out patches held at −50 mV. (A) average current (■ ± SEM) from seven different patches. Channel current drops to the noise level rapidly upon application of toxin, and shows a slow recovery to the initial current level upon toxin washout. The recovery kinetics were fitted to a single exponential with a time constant of 4.7 ± 1.7 s (B).

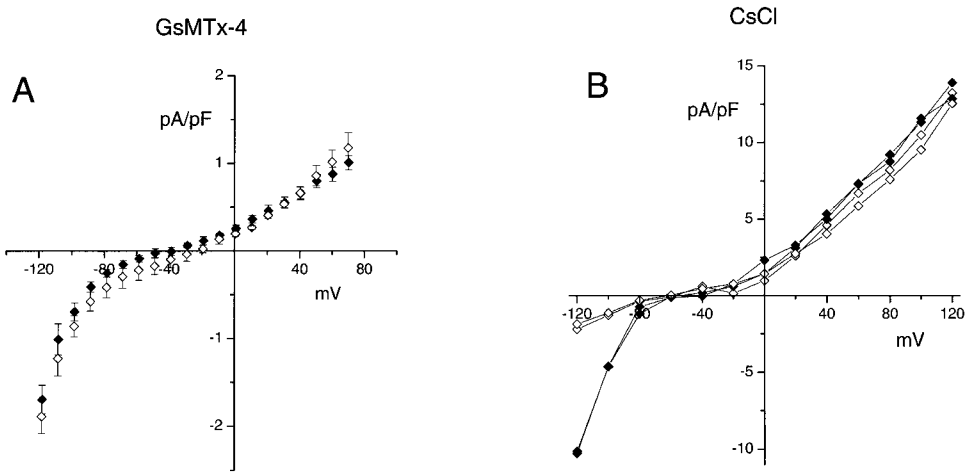

Figure 7. GsMTx-4 does not significantly affect voltage-sensitive currents. Whole-cell currents are shown from astrocytes voltage clamped using the perforated-patch technique. (A) Average whole-cell current from six cells, produced by a 600-ms ramp from −120 to 80 mV. There is no significant difference between whole-cell currents in isotonic saline (◆) and currents measured between 30 and 120 s after perfusion with 5 μM GsMTx-4 (◇). (B) Peak currents from a single cell stepped in 20-mV increments between −120 and 120 mV in the absence (◆) or presence (◇) of 5 mM CsCl. In contrast to GsMTx-4, CsCl produces a significant decrease in current at hyperpolarized potentials. After the first application of CsCl, the cell was washed and the experiment was repeated. Thus, the I-V plot shows two sets of data points for both control and CsCl.

be due to nonselective cationic SACs (Kimelberg and Kettenmann, 1990). However, a large rapidly developing DIDS-sensitive anionic current dominates the passive membrane current (Pasantes-Morales et al., 1994; Bakhramov et al., 1995). After 30-s exposure to hypotonic conditions, adult astrocytes display a similar large-conductance increase that slowly inactivated at large depolarizing voltages [compare Fig. 9 A (resting current) to B (swelling-activated current)]. During hypotonic exposure, cells were held at −50 mV before I-V test voltage steps to reduce the influence of voltage-gated Ca^{2+} channels on Ca^{2+} influx. The swelling-activated current has a large anionic component since 50 μM DIDS produced a significant reduction in current (especially at depolarized potentials) and a −33-mV shift in reversal potential (Fig. 10, $n = 6$). A residual current with a reversal potential shifted toward E_K remained. Applying 5 μM GsMTx-4 while hypotonically swelling the cell significantly reduced the peak current response at 30 s after hypotonic exposure (Fig. 9 C). After washout of GsMTx-4, a hypotonic stimulus produced larger swelling-activated currents, although less than the original control stimulus (Fig. 9 D). This reduced response after washout is not due to lingering toxin effects, since >3 min of washout separated successive hypotonic stimuli. The response to successive hypotonic exposures slowly decreased over time (Fig. 9 F, a and b), probably due to RVD mechanisms. Representative peak-current responses from two different cells displayed a roughly linear decrease in swelling-activated current (Fig. 9 F, ■). GsMTx-4 always reduced the swelling-activated current from the control response (Fig. 9 F, ◇). In light of the slowly degrading hypotonic response, to estimate the amount of GsMTx-4 block, we had to correct for the "rundown" by linear interpolation. The I-V profiles for the swelling-activated difference currents (Fig. 9 G) show a clear difference between the before (■) and after (●) responses. The percent block produced by GsMTx-4 (◇) relative to each of the control curves is shown to the right. The estimated reduction in swelling-activated current produced by 5 μM GsMTx-4 was similar at both hyperpolarizing and depolarizing potentials (∼48% at −100 mV and ∼38% at +100 mV). Furthermore, unlike DIDS, which produced a large (−33 mV) shift in reversal potential due to the specific loss of anionic current, GsMTx-4 produces almost no change in reversal potential (+2 mV, statistically indistinguishable from 0 mV).

GsMTx-4 Effects on CHF Model Ventricular Myocytes Whole-Cell Currents

Swelling-activated currents in rabbit and dog cardiac myocytes are persistently activated in CHF and may play a role in the development of congestive heart failure (Clemo and Baumgarten, 1997; Clemo et al., 1998). Both an inwardly rectifying cation selective cur-

GsMTx-4	G C L E - F W W K C N P N D D K C C R P K L K C S K L F K L - - C N F S S A
TXP5	S C V D - P Q T K C K K D S D - C C - G K L E C S S R W K W - - C V Y P S P F
SNX-482	G V D K A G C R Y M F G G - C S V N D D - C C - P R L G C H S L F S Y - - G A W D L T F S D
ω-GramTX-S1A	D C V R - F W G K C S Q T S D - C C - P H L A C K S K W P R N I C V W D G S V
Hanatoxin$_1$	E C R Y L F G G - C K T T S D - C C K - H L G C K F R D K Y - - G A W D F T F S

Figure 8. Sequence of GsMTx-4 showing homology to other ion channel peptide toxins. Cysteine motif residues are included in boxes. Dark shaded residues in the comparison peptide sequences are identical to GsMTx-4, while lighter shaded residues are similar. TXP5, K^+ channel blocker (Kaiser et al., 1994): 40% identity, 54% similarity; SNX-482, blocks E-type Ca^{2+} channels (Newcomb et al., 1998): 40% identity, 49% similarity; ω-GramTX S1A, blocks N-, P-, and Q-type Ca^{2+} channels (not L-type) (Lampe et al., 1993): 34% identical, 46% similarity; Hanatoxin, K^+ channel blocker (Swartz and MacKinnon, 1995): 28% identical, 37% similarity.

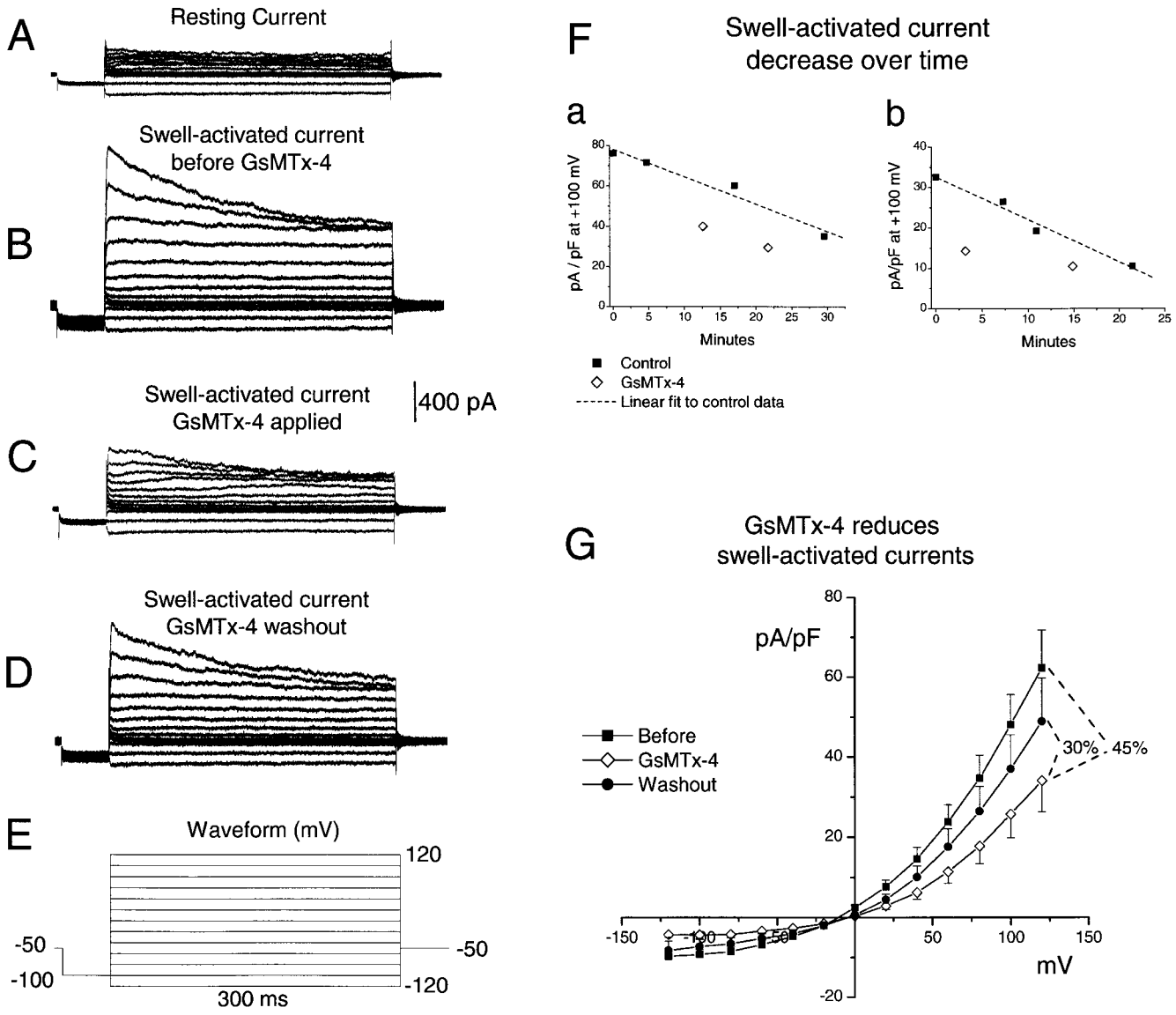

Figure 9. GsMTx-4 reduces whole-cell swelling-activated current in astrocytes exposed to hypotonic saline. Whole cell currents (A–D) from perforated patches on astrocytes. (A) Resting whole-cell currents in isotonic saline produced by the waveform shown in E (isotonic saline is normal bath saline with 80 mM NaCl replaced by 160 mM mannitol). Current scale bar is shown (right). Swelling-activated currents were recorded after the cell had been exposed for 30 s to hypotonic saline (B, isotonic saline minus 140 mM mannitol). (C) Perfusion of hypotonic saline with 5 μM GsMTx-4 produced an ~75% reduction in the peak swelling-activated current at 30 s, after subtracting resting current. Swelling currents partially recovered ~4 min after washout of GsMTx-4 (D). Peak swelling-activated currents at 100 mV (F, ■) from two different cells (a and b) decreased over successive exposures to hypotonic solution. (F, ◇) Peak currents measured during hypotonic exposures with GsMTx-4 present were reduced from the control. (G) I-V plot of the average swelling-activated peak currents from six cells measured 30–40 s after hypotonic exposure. The data points represent difference currents calculated by subtracting the resting current from hypotonic current. Control hypotonic current (■), hypotonic currents in the presence of GsMTx-4 (◇), and hypotonic currents after ~5 min of washout (●). The hypotonic current in the presence of GsMTx-4 is ~38% lower than control swell currents at +100 mV and ~48% lower at −100 mV.

rent ($I_{Cir,swell}$) and an outwardly rectifying Cl^- current ($I_{Cl,swell}$) are involved in volume regulation in cardiac myocytes. In ventricular myocytes from rabbits with aortic regurgitation-induced congestive heart failure, these two currents are constitutively activated in isotonic media (Fig. 11 A, a) and are inactivated when the cell is perfused with hypertonic saline (b). At 0.4 μM, GsMTx-4 produced a nearly complete block of the inward $I_{Cir,swell}$, but had no effect on the outward $I_{Cl,swell}$ (Fig. 11 B, c). However, whole-cell current was unaffected by GsMTx-4 when swelling-activated currents were inactivated by 1.5T hypertonic saline (Fig. 11 B, d). The difference currents in Fig. 11 C show that GsMTx-4 blocked only inward swelling-activated current [compare Fig. 11 C, $1.0T_C - 1.5T_C$ (total $I_{Cir,swell}$) with $1.0T_C - 1.0T_{Tx}$ (toxin sensitive $I_{Cir,swell}$)]. The re-

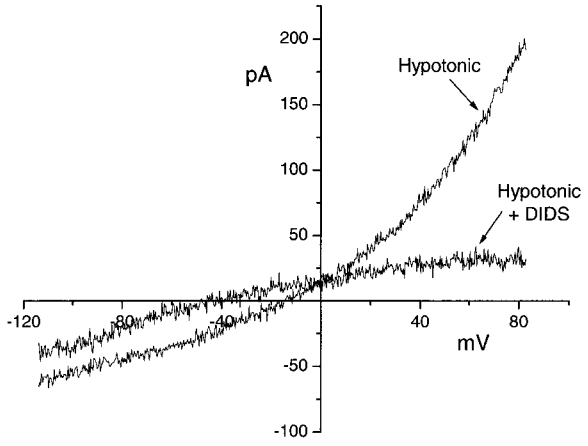

Figure 10. DIDS reduces swelling-activated currents in adult astrocytes. Whole-cell currents produced by a 600-ms ramp in voltage from −120 to 80 mV at 30 s after exposure to hypotonic saline are shown. Hypotonic and hypotonic + 50 μM DIDS difference current are shown, produced by subtracting the whole-cell current under isotonic conditions from the current observed during hypotonic exposure. A large reduction in swelling-activated current is observed at hyperpolarized potentials compared with the reduction observed at negative potentials. The reversal potential shift caused by DIDS is approximately −30 mV. The average reversal potential shift from six cells exposed to DIDS during hypotonic swelling was approximately −33 ± 3.5 mV.

maining inward current is largely $I_{Cl,swell}$. The toxin produced no further current reduction in the presence of hypertonic saline, which inactivates the swelling-activated current (Fig. 11 C, $1.5T_C - 1.5T_{Tx}$). This result again supports the specificity of GsMTx-4. When volume changes are examined (Fig. 11 D), GsMTx-4 produced a cell volume reduction that is ~40% of that produced by 1.5T hypotonic saline.

DISCUSSION

A New Tool

We have found the first specific reagent for mechanosensitive ion channels (MSCs). It is surely only a prototype, with many reagents to follow. While studies are needed to establish the cross reactivity of GsMtx-4 for different types of MSCs, as well as for cross reactivity with different types of channels, GsMtx-4 is a unique agent. It can be used to test the involvement of SACs in physiological processes in situ or in vivo. Its ability to suppress cardiac arrhythmias (Bode et al., 1999) suggests a clinical significance. Its ability to suppress cell swelling may also be clinically useful for dealing with edema. GsMtx-4 may be derivatized to make affinity columns for purifying the channel protein and for making histochemical markers to localize the channels.

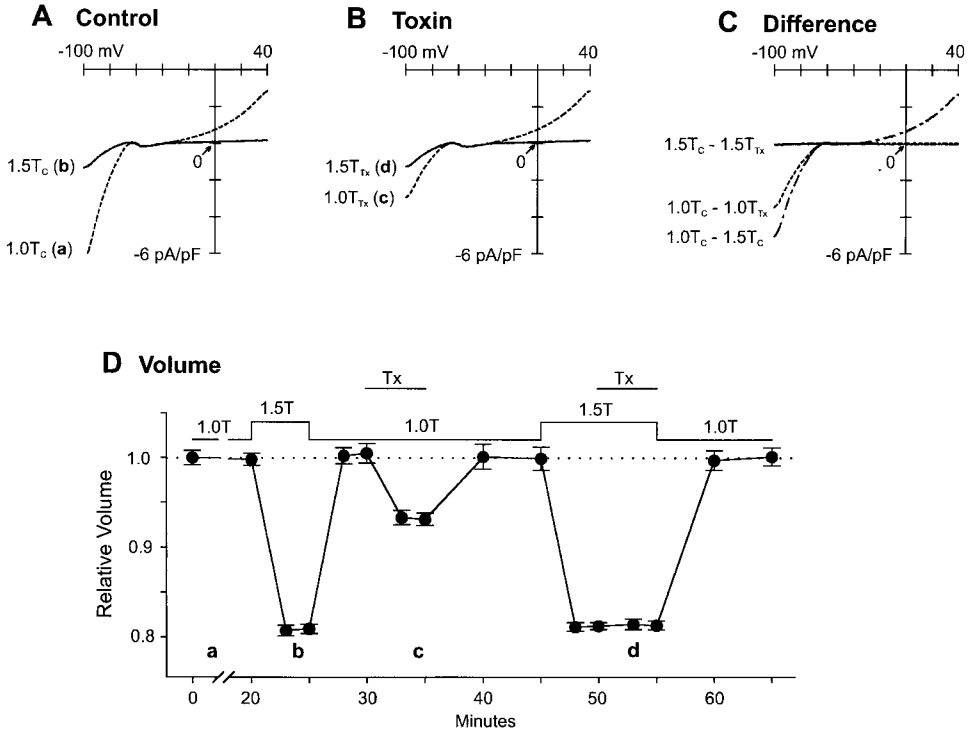

Figure 11. Ionic currents (A–C) and cell volumes (D) measured during perforated patch voltage clamp (E_{hold} = −80 mV) of ventricular myocytes from rabbits with aortic regurgitation-induced CHF. Myocytes were exposed to 1.0T and 1.5T solution in the absence [$1.0T_C$ (dashed line), $1.5T_C$ (solid line)] and presence [$1.0T_{Tx}$ (dashed line), $1.5T_{Tx}$(solid line)] of 0.4 μM GsMTx-4. (A) Osmotic shrinkage in the control solution reduced both inward and outward currents. (B) Toxin reduced the inward currents in 1.0T, but the currents in 1.5T were unaffected (compare A and B). (C) Difference currents: $1.0T_C$–$1.5T_C$ (dash-dot line), shrinkage-sensitive current due to inhibition of cationic SACs and anionic swelling currents; $1.0T_C$–$1.0T_{Tx}$ (dashed line), inwardly rectifying toxin-sensitive current. The toxin-sensitive current was similar to the Gd^{3+}-sensitive currents recorded in the same model (data not shown, Clemo and Baumgarten, unpublished observations). $1.5T_C$–$1.5T_{Tx}$ (solid line), toxin did not affect membrane currents when SACs were inhibited by osmotic shrinkage. (D) Consistent with block of ion influx via cationic SACs, toxin reduced cell volume by 7% in 1.0T solution. In contrast, cell volume was unaffected after osmotic shrinkage in 1.5T solution, conditions under which SACs are closed. I-V curves elicited by ramp clamps (28 mV/s) and cell volume data are averages from five cells. Lower case letters (a, b, c, and d) designate time of current measurements in I-V profiles.

It is surprising that GsMtx-4 can act across different tissues in similar concentrations. This implies a strong homology between the cationic SACs of these tissues and may help to define a family of channels. The teleological significance of why a rather mild tarantula venom would have the ability to block SACs in a rabbit heart or a rat brain is unclear. Perhaps insects, the spider's normal prey, have similar channels.

The mechanism of action of GsMtx-4 remains to be determined. We do know that it can act on closed channels, but we don't know if this occurs because the activation curve is shifted to higher tensions or because GsMtx-4 blocks the permeation path. These studies are now in progress.

GsMTx-4 Structure

GsMTx-4 possesses an ICK consensus cysteine motif with the basic structure defined by three cysteine pairs (C_1–C_4, C_2–C_5, and C_3–C_6) that stabilize a core region composed of a triple-stranded antiparallel β sheet (for review, see Norton and Pallaghy, 1998). Enzymatic digest fragments are currently being analyzed to confirm this structure. Examples of toxin families active against ion channels that possess ICK motifs are: the μ-agatoxins and δ-atracotoxins, which block voltage-activated Na^+ channels; the ω-agatoxins, ω-conotoxins, and ω-atracotoxins, which block voltage-gated Ca^{2+} channels; and hanatoxin, κ-conotoxin, and TXP-5, which block voltage-gated K^+ channels. GsMTx-4 shows the most sequence similarity to K^+ and Ca^{2+} channel blocking toxins from tarantula venoms, the highest being TXP-5 from the *Brachypelma smithii* tarantula, where the similarity is 54%. However, sequence homology between ICK containing peptide toxins is a poor indicator of functional similarities. For example, the N-type Ca^{2+} channel blocker ω-conotoxin MVIIA has >80% sequence similarity with P/Q-type Ca^{2+} channel blocker ω-conotoxin MVIIC, while sharing only 45% sequence similarity with the N-type Ca^{2+} channel blocker ω-conotoxin GVIA.

We have recently produced a recombinant GsMTx-4 peptide in bacteria that in initial experiments blocks SACs in outside-out patches from astrocytes. This removes the possibility of a copurified contaminant along with GsMtx-4 from raw venom.

GsMTx-4 Binding Affinity in Astrocyte and Cardiac Myocyte Assays

The equilibrium constant for toxin binding was calculated to be ~600 nM. While many peptide toxins are highly specific for their receptor, having affinities (IC_{50} or K_d) in the 0.1–100 nM range, GsMTx-4 binds 5–50× more tightly than any other antagonist tested to date on any stretch channel. It appears to be specific for cation SACs since it did not effect voltage-sensitive currents in astrocytes or $I_{Cl,swell}$ in myocytes. The complete block of $I_{Cir,swell}$ at 0.4 μM indicates that toxin affinity for its binding site in cardiac myocytes may be even stronger than in astrocytes. Preliminary results from atrial-induced fibrilation experiments with Langendorff-perfused rabbit hearts suggest that GsMTx-4 doesn't block normal electrical activity of the heart (eliminating many possible sites of cross reactivity) and the toxin may have a higher affinity for these cells in situ (Bode et al., 1999). In these studies, 0.17 μM GsMtx-4 was capable of inhibiting the atrial fibrillation associated with dilatation.

Changes in SAC Properties between Cell-attached and Outside-Out Patches

The properties of SACs in activated adult astrocytes, including ion selectivity, conductance, inward rectification, and adaptation, are similar to cation-selective SACs observed in other systems (Yang and Sachs, 1993). Outside-out patches were used in only one previous study to determine the effects of Gd^{3+} (Yang and Sachs, 1989) on SACs in *Xenopus* oocytes. However, in that report, the effects of outside-out formation on channel properties was not rigorously assessed because it was difficult to maintain activity in the patch. Patches from most cell types rapidly lose SAC activity with excision.

In the adult astrocytes, SAC adaptation is lost during outside-out patch formation, or if >10 mmHg suction is used for cell-attached seal formation. At voltages where adaptation should rapidly reduce channel P_o (−50 mV), in outside-out patches we observed a delayed activation instead (Figs. 1 B, +100 mV average current, and 5 A, average current). This selective loss of adaptation is similar to the two stages of decoupling described by Hamill and McBride (1992) in *Xenopus* oocytes. The mechanisms for these changes in gating as a function of patch history remain to be determined.

However, the intrinsic permeation properties of the channels, such as channel conductance, rectification, and ion selectivity, seem less likely to be affected by cytoskeletal attachments and appear less sensitive to patch history, as shown in Fig. 1, C and D. Even while more pressure/suction is required over time to activate the channel in either configuration (decoupling of the tonic gating element), channel conductance and rectification remain unchanged. Furthermore, although ion selectivity was not rigorously compared between the two patch configurations, channel conductance was 46 pS with 130 mM CsCl substituted for KCl in the pipette, demonstrating the channel is nonselective for cations in the cell-attached mode. Thus, outside-out patches are an adequate representation of the activity in cell-attached patches and a much more flexible preparation for screening.

SAC Activity during Astrocyte Cell Swelling

The sensory processes for RVD have not been determined, but these experiments strongly suggest that cationic SACs play a role. While dilution of internal K^+ and an increase Na^+ flux could contribute to membrane depolarization, this is an ineffective stimulus under voltage clamp and it has been demonstrated in multiple studies on different cell types that an increase in anionic current is the major contributor to membrane depolarization during hypotonic swelling (Pasantes-Morales et al., 1994; Bakhramov et al., 1995). The trigger for the volume-activated anion current is still unclear. In our adult astrocytes, anion current accounts for nearly the entire reversal potential shift that occurs after hypotonic exposure. GsMTx-4 produces a 40–50% reduction in swelling-activated anion current, suggesting that cationic SACs contribute to activation of the current. However, in contrast to DIDS blockade of the anionic current, the reduction in swelling-activated current produced by GsMTx-4 showed no change in reversal potential. This could be due to a reduction of SAC cation current or an overall decrease in all swelling-activated currents. Dose response studies with GsMtx-4 are in order.

Although anion current dominates the whole-cell conductance during RVD, swelling-activated K^+ currents that generally develop more slowly are rate limiting for Cl^- efflux. Increasing the cation flux with gramicidin can circumvent the rate-limiting effect of the slowly increasing K^+ current (Pasantes-Morales et al., 1994). Activation of cation-selective SACs, like gramicidin, would increase the flux of cations (increasing Cl^- efflux), and thus the rate of RVD.

RVD in astrocytes has been reported to be a Ca^{2+}-dependent process (O'Connor and Kimelberg, 1993; Bender et al., 1994). Thus, GsMTx-4 may block Ca^{2+} influx through SACs' reducing Ca^{2+}-sensitive swelling-activated currents. Contributions to Ca^{2+} influx through voltage-gated Ca^{2+} channels were reduced by clamping the cell at −50 mV before recording the whole-cell currents. A number of swelling-activated anion currents have been identified that are induced by secondary messenger systems such as Ca^{2+}, calmodulin, and various kinases. Although it has been shown that the DIDS-sensitive Cl^- current is not Ca^{2+} dependent in neonatal astrocytes (Pasantes-Morales et al., 1994; Bakhramov et al., 1995; Crepel et al., 1998), Ca^{2+}-activated Cl^- currents are partially responsible for the anion efflux during RVD in Ehrlich ascite cells (Hoffmann et al., 1986; Lambert et al., 1989). It is possible that anion currents between neonatal and adult rat astrocytes may differ, especially since different SACs are observed between separate neonatal preparations (Bowman et al., 1992; Islas et al., 1993) and adult astrocytes. Further characterization of GsMTx-4's effects on membrane currents and Ca^{2+} influx is required to more clearly define the role of SACs in RVD.

GsMTx-4 Effect on Rabbit CHF-model Cardiac Myocytes

In cardiac myocytes, stretch/swell-induced currents may play a critical role in the development of dysrhythmias and hypertrophy, and may alter contractile function. Cationic ($I_{Cir,swell}$) and anionic ($I_{Cl,swell}$) swelling-activated currents have been identified in hypotonically swollen rabbit cardiac myocytes (Clemo and Baumgarten, 1997), and these may also be activated by the cell swelling that occurs during ischemia. Cardiac myocytes isolated from dog hearts with Tachychardia-induced CHF (Clemo et al., 1998) maintain a cell volume 1.24× greater than normal cells. Both $I_{Cir,swell}$ and $I_{Cl,swell}$ are constitutively active in these CHF-model cardiomyocytes under isotonic conditions. Moreover, swelling-activated currents are persistently active in rabbit myocytes from an aortic regurgitation model. GsMTx-4 at 0.4 μM specifically blocked $I_{Cir,swell}$ in CHF cardiomyocytes. The cation current $I_{Cir,swell}$ might represent activity of cationic SACs. They are both inwardly rectifying, blocked by Gd^{3+}, and poorly selective for cations ($P_K/P_{Na} = 6$).

The fact that GsMTx-4 blocks SACs in rat astrocytes and $I_{Cir,swell}$ (properties similar to cation-selective SACs) in rabbit cardiac myocytes suggests that many cell types incorporate SACs as part of the volume-regulatory process. Furthermore, the common toxin sensitivity suggests that at least some cation channels opened by direct mechanical stimulation are also opened by cell swelling. GsMTx-4 will be useful in elucidating the function of SACs in a variety of systems under physiologically normal and stressed conditions.

This work was funded by grants to Dr. Frederick Sachs from the National Institutes of Health, the United States Army Research Office, and NPS Pharmaceuticals, Inc. Studies on myocytes were supported by HL46764 to Dr. Baumgarten.

Submitted: 9 July 1999
Revised: 2 March 2000
Accepted: 6 March 2000

REFERENCES

Bakhramov, A., C. Fenech, and T.B. Bolton. 1995. Chloride current activated by hypotonicity in cultured human astrocytoma cells. *Exp. Physiol.* 80:373–389.

Bascur, L., I. Yevenes, and P. Barja. 1982. Effects of *Loxosceles laeta* spider venom on blood coagulation. *Toxicon*. 20:795–796.

Ben-Tabou, S., E. Keller, and I. Nussinovitch. 1994. Mechanosensitivity of voltage-gated calcium currents in rat anterior pituitary cells. *J. Physiol*. 476:29–39.

Bender, A.S., L.L. Mantelle, and M.D. Norenberg. 1994. Stimulation of calcium uptake in cultured astrocytes by hypoosmotic stress: effect of cyclic AMP. *Brain Res*. 645:27–35.

Bender, A.S., A. Schousboe, W. Reichelt, and M.D. Norenberg. 1998. Ionic mechanisms in glutamate-induced astrocyte swelling: role of K^+ influx. *J. Neurosci. Res*. 52:307–321.

Biagi, B.A., and J.J. Enyeart. 1990. Gadolinium blocks low- and high-threshold calcium currents in pituitary cells. *Am. J. Physiol.* 259:C515–C520.

Bode, F., F. Sachs, and M.R. Franz. 1999. Atrial fibrillation is inhib-

ited by a peptide from spider venom that blocks stretch activated ion channels. *Circulation*. 100:1784. (Abstr.)

Bowman, C.L., J.P. Ding, F. Sachs, and M. Sokabe. 1992. Mechanotransducing ion channels in astrocytes. *Brain Res.* 584:272–286.

Bowman, C.L., and J.W. Lohr. 1996. Mechanotransducing ion channels in C6 glioma cells. *Glia.* 18:161–176.

Chamberlin, M.E., and K. Strange. 1989. Anisosmotic cell volume regulation: a comparative view. *Am. J. Physiol.* 257:C159–C173.

Chen, Y., S.M. Simasko, J. Niggel, W.J. Sigurdson, and F. Sachs. 1996. Ca^{2+} uptake in GH3 cells during hypotonic swelling: the sensory role of stretch-activated ion channels. *Am. J. Physiol.* 270: C1790–C1798.

Christensen, O. 1987. Mediation of cell volume regulation by Ca^{2+} influx through stretch-activated channels. *Nature.* 330:66–68.

Clemo, H.F., and C.M. Baumgarten. 1997. Swelling-activated Gd^{3+}-sensitive cation current and cell volume regulation in rabbit ventricular myocytes. *J. Gen. Physiol.* 110:297–312.

Clemo, H.F., B.S. Stambler, and C.M. Baumgarten. 1998. Persistent activation of a swelling-activated cation current in ventricular myocytes from dogs with tachycardia-induced congestive heart failure. *Circ. Res.* 83:147–157.

Crepel, V., W. Panenka, M.E. Kelly, and B.A. MacVicar. 1998. Mitogen-activated protein and tyrosine kinases in the activation of astrocyte volume-activated chloride current. *J. Neurosci.* 18:1196–1206.

Elinder, F., P. Arhem. 1994. The modulatory site for the action of gadolinium on surface charges and channel gating. *Biophys. J.* 67: 71–83.

Fontana, A. 1972. Modification of tryptophan with BNPS-Skatole (2-2-nitrophenylsulfenyl)-3-methyl-3-bromoindolenine). *In* Methods in Enzymology. Vol. 25, part B. S.P. Colowick, and N.O. Kaplan, editors. Academic Press, Inc., New York, NY. 419–423.

Hamill, O.P., and D.W. McBride. 1996. The pharmacology of mechanogated membrane ion channels. *Pharmacol. Rev.* 48:231–252.

Hamill, O.P. and D.W. McBride, Jr. 1992. Rapid adaptation of single mechanosensitive channels in *Xenopus* oocytes. *Proc. Natl. Acad. Sci. USA.* 89:7462–7466.

Hoffmann, E.K., I.H. Lambert, and L.O. Simonsen. 1986. Separate, Ca^{2+}-activated K^+ and Cl^- transport pathways in Ehrlich ascites tumor cells. *J. Membr. Biol.* 91:227–244.

Hoffmann, E.K., and L.O. Simonsen. 1989. Membrane mechanisms in volume and pH regulation in vertebrate cells. *Physiol. Rev.* 69:315–381.

Horn, R., and A. Marty. 1988. Muscarinic activation of ionic currents measured by a new whole-cell recording method. *J. Gen. Physiol.* 92:145–159.

Hu, H., and F. Sachs. 1997. Stretch-activated ion channels in the heart. *J. Mol. Cell. Cardiol.* 29:1511–1523.

Islas, L., H. Pasantes-Morales, and J.A. Sanchez. 1993. Characterization of stretch-activated ion channels in cultured astrocytes. *Glia.* 8:87–96.

Jorgensen, F., and H. Ohmori. 1988. Amiloride blocks the mechano-electrical transduction channel of hair cells of the chick. *J. Physiol.* 403:577–588.

Kaiser, I.I., P.R. Griffin, S.D. Aird, S. Hudiburg, J. Shabanowitz, B. Francis, T.R. John, D.F. Hunt, and G.V. Odell. 1994. Primary structures of two proteins from the venom of the Mexican red knee tarantula (*Brachypelma smithii*). *Toxicon.* 32:1083–1093.

Kimelberg, H.K. 1995. Current concepts of brain edema. Review of laboratory investigations. *J. Neurosurg.* 83:1051–1059.

Kimelberg, H.K., E. Anderson, and H. Kettenmann. 1990. Swelling-induced changes in electrophysiological properties of cultured astrocytes and oligodendrocytes. II. Whole-cell currents. *Brain Res.* 529:262–268.

Kimelberg, H.K., and H. Kettenmann. 1990. Swelling-induced changes in electrophysiological properties of cultured astrocytes and oligodendrocytes. I. Effects on membrane potentials, input impedance and cell–cell coupling. *Brain Res.* 529:255–261.

Kluesener, B.G. Boheim, H. Liss, J. Engelberth, and E.W. Weiler. 1995. Gadolinium-sensitive, voltage-dependent calcium release channels in the endoplasmic reticulum of a higher plant mechanoreceptor organ. *EMBO (Eur. Mol. Biol. Organ.) J.* 14:2708–2714.

Lambert, I.H., E.K. Hoffmann, and F. Jorgensen. 1989. Membrane potential, anion and cation conductances in Ehrlich ascites tumor cells. *J. Membr. Biol.* 111:113–131.

Lampe, R.A., P.A. Defeo, M.D. Davison, J. Young, J.L. Herman, R.C. Spreen, M.B. Horn, T.J. Mangano, and R.A. Keith. 1993. Isolation and pharmacological characterization of omega-grammotoxin SIA, a novel peptide inhibitor of neuronal voltage-sensitive calcium channel responses. *Mol. Pharmacol.* 44:451–460.

Lane, J.W., D. McBride, and O.P. Hamill. 1991. Amiloride block of the mechanosensitive cation channel in *Xenopus* oocytes. *J. Physiol.* 441:347–366.

Langan, T.J., R.J. Plunkett, H. Asada, K. Kelly, and P. Kaseloo. 1995. Long-term production of neurotrophic factors by astrocyte cultures from hemiparkinsonian rat brain. *Glia.* 14:174–184.

Langton, P.D. 1993. Calcium channel currents recorded from isolated myocytes of rat basilar artery are stretch sensitive. *J. Physiol.* 471:1–11.

Magid, N.M., M.S. Young, D.C. Wallerson, R.S. Goldweit, J.N. Carter, R.B. Devereux, and J.S. Borer. 1988. Hypertrophic and functional response to experimental chronic aortic regurgitation. *J. Mol. Cell Cardiol.* 20:239–246.

Narasimhan, L., J. Singh, C. Humblet, K. Guruprasad, and T. Blundell. 1994. Snail and spider toxins share a similar tertiary structure and "cystine motif". *Nat. Struct. Biol.* 1:850–852.

Newcomb, R., B. Szoke, A. Palma, G. Wang, X. Chen, W. Hopkins, R. Cong, J. Miller, L. Urge, K. Tarczy-Hornoch, et al. 1998. Selective peptide antagonist of the class E calcium channel from the venom of the tarantula *Hysterocrates gigas*. *Biochemistry.* 37:15353–15362.

Norton, R.S., and P.K. Pallaghy. 1998. The cystine knot structure of ion channel toxins and related polypeptides. *Toxicon.* 36:1573–1583.

O'Connor, E.R., and H.K. Kimelberg. 1993. Role of calcium in astrocyte volume regulation and in the release of ions and amino acids. *J. Neurosci.* 13:2638–2650.

Paoletti, P., and P. Ascher. 1994. Mechanosensitivity of NMDA receptors in cultured mouse central neurons. *Neuron.* 13:645–655.

Pasantes-Morales, H. 1996. Volume regulation in brain cells: cellular and molecular mechanisms. *Metab. Brain Dis.* 11:187–204.

Pasantes-Morales, H., R.A. Murray, L. Lilja, and J. Moran. 1994. Regulatory volume decrease in cultured astrocytes. I. Potassium- and chloride-activated permeability. *Am. J. Physiol. Cell Physiol.* 266:C165–C171.

Perez, F., S. Luca, P. DaSilva, and R. Bertani. 1996. Systematic revision and cladistic analysis of Theraphosinae. *Mygalomorph.* 1:33–68.

Ruknudin, A., F. Sachs, and J.O. Bustamante. 1993. Stretch-activated ion channels in tissue-cultured chick heart. *Am. J. Physiol. Circ. Physiol.* 264:H960–H972

Sachs, F. 1988. Mechanical transduction in biological systems. *Crit. Rev. Biomed. Eng.* 16:141–169.

Sachs, F. 1992. Stretch sensitive ion channels: an update. *In* Sensory Transduction. D.P. Corey and S.D. Roper, editors. Rockefeller University Press. New York, NY. 241–260.

Sachs, F., and C. Morris. 1998. Mechanosensitive ion channels in non specialized cells. *In* Reviews of Physiology and Biochemistry and Pharmacology. M.P. Blaustein, R. Greger, H. Grunicke, R. Jahn, L.M. Mendell, A. Miyajima, D. Pette, G. Schultz, and M.

Schweiger, editors. Springer Verlag, Berlin, Germany. 1–78.
Sarkadi, B., and J.C. Parker. 1991. Activation of ion transport pathways by changes in cell volume. *Biochim. Biophys. Acta.* 1071:407–427.
Silberberg, S.D., and K.L. Magleby. 1997. Voltage-induced slow activation and deactivation of mechanosensitive channels in *Xenopus* oocytes. *J. Physiol.* 505:551–569.
Small, D.L., and C.E. Morris. 1995. Pharmacology of stretch-activated K^+ channels in *Lymnaea* neurones. *Br. J. Pharmacol.* 114: 180–186.
Sontheimer, H. 1992. Astrocytes, as well as neurons, express a diversity of ion channels. *Can. J. Physiol. Pharmacol.* 70:S223–S238
Swartz, K.J., and R. MacKinnon. 1995. An inhibitor of the Kv2.1 potassium channel isolated from the venom of a Chilean tarantula. *Neuron*. 15:941–949.
Tazaki, M., and T. Suzuki. 1998. Calcium inflow of hamster Merkel cells in response to hyposmotic stimulation indicate a stretch-activated ion channel. *Neurosci. Lett.* 243:69–72.
Vandenberg, J.I., S.A. Rees, A.R. Wright, and T. Powell. 1996. Cell swelling and ion transport pathways in cardiac myocytes. *Cardiovasc. Res.* 32:85–97.
Wilson, K.J. 1989. Methods in protein sequence analysis: proceedings of the 7th international conference, Berlin, July 3–8, 1988. B. Wittmann-Leibold, editor. Springer-Verlag, New York, NY. 310–330.
Yang, X.C., and F. Sachs. 1989. Block of stretch-activated ion channels in *Xenopus* oocytes by gadolinium and calcium ions. *Science.* 243:1068–1071.
Yang, X.C., and F. Sachs. 1993. Mechanically sensitive, non-selective, cation channels. *In* Non-Selective Ion Channels. D. Siemen and J. Hescheler, editors. Springer-Verlag, Heidelberg, Germany. 79–92.